WILEY | Hindawi

Research Article

Quantitative Evaluation of the Transmission and Removal of Harmful Smoke Particles in the Operating Room: Full-Scale Experimental and Numerical Study

Zhijian Liu [iD],[1] Zheng Zhang [iD],[1] Jiabin Lv,[1] Juntao Ma,[1] Guangpeng Yao,[1] Junzhou He,[1] and Guoqing Cao[2]

[1]*Department of Power Engineering, North China Electric Power University, Baoding, Hebei 071003, China*
[2]*Institute of Building Environment and Energy, China Academy of Building Research, Beijing 100013, China*

Correspondence should be addressed to Zhijian Liu; zhijianliu@ncepu.edu.cn

A large amount of surgical smoke in electrosurgery seriously deteriorates the clean environment of the operating room and can potentially harm medical staff and patients. Exploring the distribution and removal of indoor particulate matter and selecting efficient ventilation patterns are effective ways to control harmful smoke. Therefore, in this study, we combined simulations and full-scale experiments to quantitatively explore the high-concentration spatial regions of particles and compared three ventilation patterns: vertical laminar airflow (VLAF), horizontal laminar airflow (HLAF), and hybrid ventilation, wherein unidirectional airflow (UDAF) was applied to the operating table along with peripheral mixing (UDAF + mixing). We found that simple laminar flow ventilation was significantly affected by the equipment layout and air change rate (air changes per hour; ACH), and the smoke particles were distributed in large amounts in the operating area and could not be removed completely. Conversely, hybrid ventilation can work effectively, and the optimal ACH is approximately 60, which can remove nearly 72% of smoke particles. The airflow distribution in the operating room is also an important factor affecting the distribution and removal of smoke particles. Therefore, medical staff should avoid prolonged exposure to areas with high particle concentrations and particle removal paths.

1. Introduction

Air pollution control in the operating room is a basic requirement to maintain the health of patients and medical staff [1, 2]. However, in many surgical procedures, high-frequency electric knives cut tissue by heating and burning, resulting in a large amount of surgical smoke [3–5]. These particles, which carry harmful substances, are often considered a major contamination source during surgery [6]. In several studies, electrosurgical particles have been found to be susceptible to airflow and quickly spread far from the wound [2, 7], spreading disease to healthcare workers through viral and bacterial pathogens in the smoke particles [8, 9]. Therefore, it is essential to study the ventilation patterns and the distribution and removal of smoke particles

during the operation process to provide effective suggestions for maintaining a clean operating room environment.

Several standards and guidelines have addressed surgical smoke exposure. The Occupational Safety and Health Administration (OSHA) states that nearly half a million healthcare workers are exposed to electrosurgical smoke in operating rooms [10]. Although healthcare workers take precautions during surgery, regular masks can only protect against particles larger than 0.5 microns. A large number of smoke particles are fine particles with a diameter of about 0.3 microns or even smaller ultrafine particles [11]. Exposure and inhalation of surgical smoke can lead to acute adverse effects and severe health risks for patients and staff [3, 12, 13]. Many studies have shown the presence of dangerous substances in surgical smoke, including carcinogens,

harmful chemicals, bacteria, and viruses, and long-term exposure can lead to eye irritation, headaches, nausea, weakness, and even the risk of cancer [14]. Currently, OSHA standards do not require ventilation and filtration systems, nor do they set specific particulate limits for controlling smoke from electrosurgery [10]. Increasing studies have focused on the properties and hazards of volatile organic compounds in smoke particles, but little attention has been paid to intraoperative particle distribution and concentration monitoring.

Ensuring high air quality in operating rooms is essential for reducing smoke particles and protecting the health of medical staff and patients. Among them, the use of ventilation patterns is the most effective way to control the risk of cross-infection [15–19]. Laminar airflow (LAF) ventilation is currently widely used in operating rooms and other clean rooms to effectively create a sterile environment around patients and healthcare staff [20–22]. Numerous studies have experimentally or numerically demonstrated that LAF is superior to mixed ventilation in reducing the risk of patient exposure [23]. Hansen et al. experimentally studied the effect of ventilation on the transport of fine and ultrafine particles in the operating room [15]. The results show that the LAF system is superior to the turbulent mixed airflow system in removing particles. Although LAF is used as a general design requirement, its operation remains flawed, and there is a risk of cross-infection between patients and healthcare staff [24]. Previous studies have shown that the direction of vertical laminar airflow (VLAF) is easily affected by surgical lamp blockage [25]. Additionally, the thermal plume and updraft caused by the temperature difference between the body surface and the surrounding environment greatly reduce the effect of the vertical airflow created by the VLAF on particle removal [23, 26]. As another form of laminar ventilation, horizontal laminar airflow (HLAF) greatly attenuates the influence of operating lights and medical staff on the concentration of particulate matter in the operating area. However, there are higher requirements in terms of the design parameters and operating room layout, and the stability is not guaranteed [27]. In recent years, owing to the complexity of the operating environment, more medical equipment has been used in the operating room, forming a hybrid between the ordinary operating room and the diagnostic room. Different forms of ventilation (unidirectional airflow (UDAF) on the operating table and a peripheral hybrid ventilation system) were used in each area. Romano et al. examined air pollution in operating rooms during surgery using this ventilation system. Their results show that operating rooms equipped with this system can better dilute and eliminate air pollution [3]. Different ventilation patterns have their own advantages and disadvantages in maintaining a clean environment in the operating room. Therefore, it is important to compare the spatial concentration distribution of smoke particles in an operating room under different ventilation patterns. Meanwhile, increasing research has focused on reducing the risk of wound infection during surgery [28, 29], and little attention has been paid to the effects of particulate matter on healthcare workers. Notably, cross-infection is bidirectional; thus, detailed comparisons and analyses of particulate concentrations near patients and healthcare workers are also of interest.

Air changes per hour (ACH) are an important factor affecting the ventilation effect of different ventilation systems [28, 30]. Romano et al. studied the relationship between ACH and particulate matter concentrations in the operating room, and an increase in ACH tended to reduce the ambient particulate matter concentrations [31]. A previous study showed that ACH in the operating room had a great impact on the indoor airflow distribution and the particulate matter distribution in the operating area and surrounding areas [32]. Another study showed that ACH had a greater impact on the distribution of bioaerosols in the surgical area than that in the temperature conditions [33]. Therefore, it is important to consider the influence of ACH on the distribution of intraoperative smoke particles.

The migration rule, spatial concentration distribution, and removal efficiency of smoke particles under the three ventilation patterns were studied in a standard class I operating room. In the experiment, electrosurgical equipment was used to cut through pork tissue to create a smoky environment. The operating area is an important part of the operating room. Therefore, the local pollutant exposure index and spatial concentration were used to quantitatively analyse the spatial concentration distribution and changes in particles near patients and medical staff in the operating area under different ACH values for the three ventilation patterns. The removal efficiency of particulate matter in the operating room was measured and compared. Our results can guide the prevention of surgical smoke and effectively reduce the harm caused by smoke particles to the surgical staff.

2. Experiment Settings and Methodology

2.1. Physical Model. As shown in Figure 1(d), a standard class I operating room environmental test chamber has dimensions of $7.2 \times 6.3 \times 3$ m ($L \times W \times H$). The operating room has three air supply forms: ceiling air supply, side-wall air supply, and slit air supply. In the middle of the ceiling, there were eight air outlets with a size of 1.345×0.6225 m and a HEPA filter. Eight air supply outlets with a size of 1.3×0.35 m were present around the ceiling, and an entire air supply outlet with a size of 3.05×2.5 m was located on the side wall opposite the door. The left and right sides of the room were, respectively, equipped with four exhaust vents with a size of 0.9×0.35 m, and the lower edge of each exhaust outlet was 0.15 m away from the ground.

The basic facilities in the operating room adhere to the standard of a typical level I operating room, including a single-arm mechanical surgical tower, an operating table, two operating lights, an instrument table, electric surgical equipment, and some common equipment. Additionally, the operating room staff comprised one patient and four medical staff members, as shown in Figure 1. This arrangement is equivalent to that commonly used in abdominal or visceral surgeries. The height of the mannequin was 1.75 m, and the heat load of the mannequin was adapted to the level of individual activity.
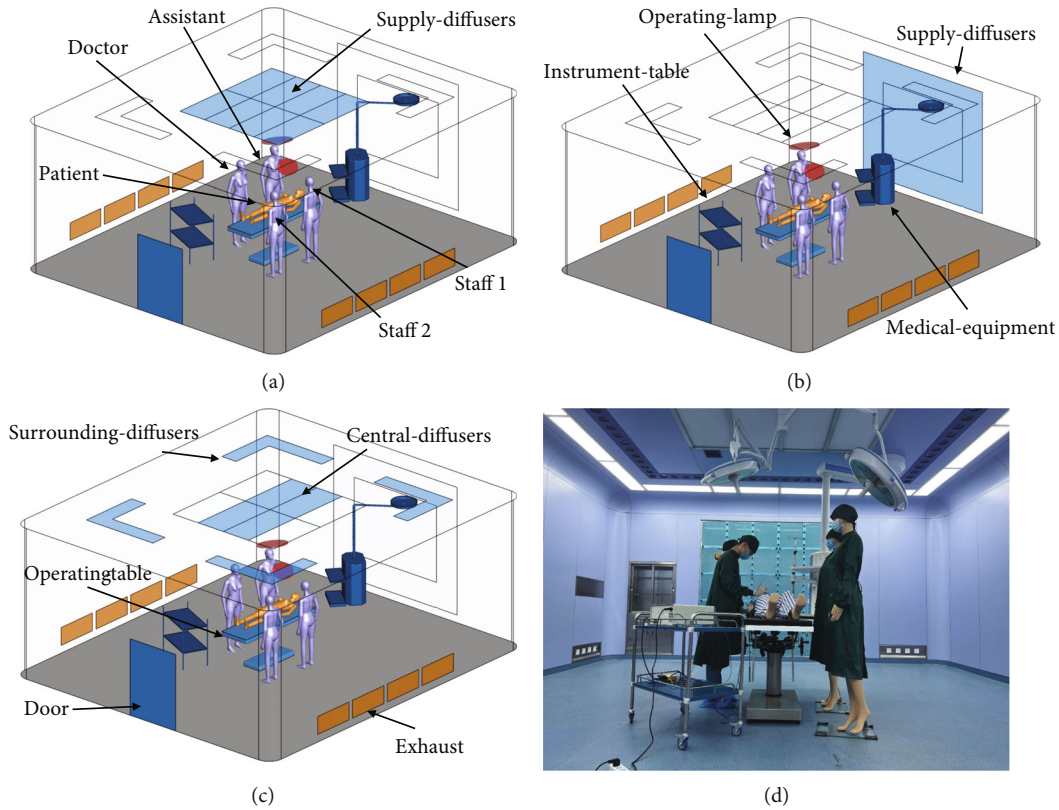
FIGURE 1: Operating room model and environment room layout. (a) OR 1 equipped with VLAF system; (b) OR 2 equipped with HLAF system; (c) OR 3 equipped with UDAF + mixing system; (d) environment room layout.

2.2. Case Study and Instrumentation. The layout of the operating room equipped with the VLAF, HLAF, and UDAF + mixing ventilation systems is shown in Figures 1(a)–1(c), and the specific design parameters of each ventilation system are listed in Table 1. The experimental equipment and parameters are presented in Table 2. Notably, the ACH in the UDAF + mixing system room was 60; however, the ACH in the surgical area was higher than that in the surrounding area.

2.3. Experimental Method. Studies using pig tissue models to assess tissue damage during electrosurgical procedures have found no differences between pig tissue models and human tissue samples [11, 34]. Therefore, in this study, pork tissue was used instead of human tissue for high-frequency electric knife-cutting experiments. To simulate most surgical situations, we used the cutting mode of monopole electrotomy, which is most commonly used in surgery, to study the distribution of smoke particles in the operating room. Figure 2 shows the layout of the equipment and the generation of smoke particles in the experiment.

Three particle monitoring points were set up in the operating room: S1, S2, and S3, as shown in Figure 3. S1 was placed 1.65 m from the floor to measure the change in the particulate matter concentration in the respiratory area of the doctor. Similarly, S2 was placed 0.8 m from the floor to measure the change in particulate matter concentration in the respiratory area of the patient. Point S3 is located near the outlet, 0.2 m above the ground. The particle concentra-

tion per second at each measurement point was determined using a handheld PGM-300 particle counter.

To reduce the influence of background concentration on the measurement results, the ventilation system of the operating room was opened for at least 2 h before each experiment until the concentration at each measurement point was stable. The prepared fresh pork was placed on the patient's abdomen, which was slightly close to the attending physician. The patient lay flat on the operating table, 0.8 m above the ground. The particle counters were arranged at the smoke detection points, as shown in Figure 3. The simulation experiment was conducted using electric surgical equipment with an electric cutting power of 45 W. To measure the background concentration and eliminate environmental interference, the particle counter was turned on 5 min before the formal experiment began and then turned off 5 min after the experiment ended. The total duration of the formal surgical experiment was 15 min. The first 10 min was the surgical cutting time, and the last 5 min was the evacuation time of the surgical smoke. During the experiment, the electric knife was used to cut the tissue in a uniform linear manner. A TSI330 aerodynamic particle analyser was used to sample and record the source concentration and particle size distribution of the surgical smoke for subsequent analysis.

3. Computational Fluid Dynamic Methodology

3.1. Airflow Phase Simulation. In this study, the renormalization group (RNG) k-ε turbulence model in the analysis

TABLE 1: Properties of the operating room with three ventilation schemes.

Ventilation	Supply	Area (m^2)	Operating inflow velocity (m/s)	ACH
VLAF	Top	6.7	0.4	70
HLAF	Flank	7.6	0.35	70
UDAF + mixing	Central + surrounding	3.36 + 3.64	0.4 + 0.25	60

TABLE 2: Experimental equipment and its parameters.

| Instrumentation	Parameter
TSI, model 9565 anemometer	Measuring range of 0–30 m/s, accuracy 3%.
PGM300 laser dust particle counter	Measuring range 1–10 μm, sampling flow 2.83 L/min, and measuring accuracy 3%.
TSI 3330 optical particle size meter	Measuring range 0.3-10 μm, sampling flow rate 1 L/min.
ZG300 high-frequency electric knife	The single-pole power range of 0-300 W, the bipolar power range of 0-100 W, and the operating frequency of 500 KHz.
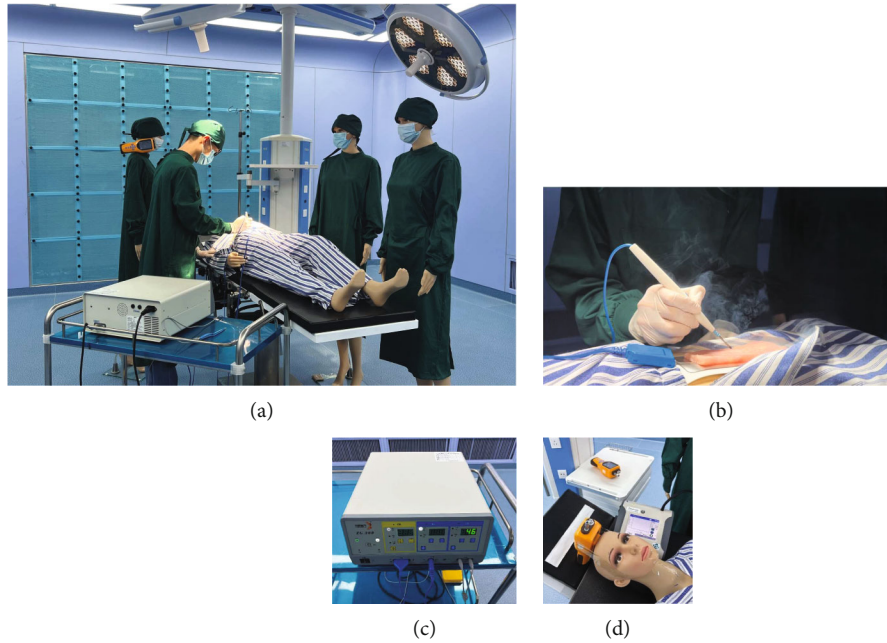
FIGURE 2: (a) Configuration of operating room. (b) High-frequency electric knife cutting. (c) High-frequency electrotome equipment. (d) Laser dust particle counter and optical particle size meter.

of systems (ANSYS) FLUENT 2020R2 was used to simulate the fluid flow. According to previous studies, the RNG k-ε model is suitable for indoor airflow simulation [35–37]. The coupling of the pressure and velocity fields was realised using the Semi-Implicit Method for Pressure Linked Equations-Consistent (SIMPLEC) algorithm. The second-order upwind discrete scheme was used for the momentum, energy, turbulent kinetic energy (k), and dissipation rate of the turbulent kinetic energy (ε). The time discrete analysis of the transient term was conducted using the second-order implicit scheme, which ensures accuracy and improves calculation speed. An enhanced wall treatment was applied near the turbulent wall. In terms of the boundary conditions, the velocity inlet was adopted, and the temperature was 294.15 K. The outlet is the pressure outlet, whose pressure value is 10 Pa. The heating load of the room was primarily supplied by air supply at a certain temperature (21°C). The surface area of the medical staff was 1.49 m^2. The patient was set at a constant temperature of 27.4°C, and the heat flux of the medical staff was 115 W/m^2. The heat fluxes of the instrument table, surgical tower, and surgical lamp were set at 150, 200, and 200 W/m^2. The remaining surfaces were set as adiabatic. The physical process of indoor radiation was not simulated in this study.
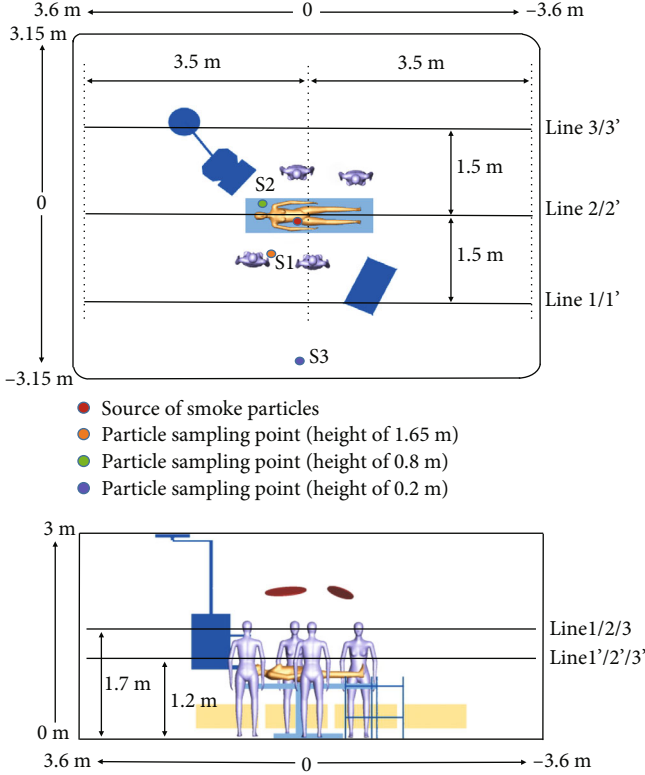
Figure 3: Location of anemometer, smoke particle concentration sampling point and surgical site.

The RNG k-ε model is derived using a statistical method called RNG theory and is expressed as follows:

$$\frac{\partial(\rho k)}{\partial t} + \frac{\partial(\rho k u_i)}{\partial x_i} = \frac{\partial}{\partial x_j}\left[\left(\mu + \frac{\mu_t}{\sigma_k}\right)\frac{\partial k}{\partial x_j}\right] + P_k - \rho\varepsilon,$$

$$\frac{\partial(\rho\varepsilon)}{\partial t} + \frac{\partial(\rho\varepsilon u_i)}{\partial x_i} = \frac{\partial}{\partial x_j}\left[\left(\mu + \frac{\mu_t}{\sigma_\varepsilon}\right)\frac{\partial \varepsilon}{\partial x_j}\right] + C_{1\varepsilon}\frac{\varepsilon}{k}P_k - C_{2\varepsilon}^*\rho\frac{\varepsilon^2}{k},$$

$$C_{2\varepsilon}^* = C_{2\varepsilon} + \frac{C_\mu \eta^3(1 - \eta/\eta_0)}{1} + \beta\eta^3,$$

(1)

where $\eta = SK/\varepsilon$ and $S = \sqrt{2S_{ij}S_{ij}}$, k is the turbulent kinetic energy per unit mass, and ε is the turbulent dissipation rate.

3.2. Particle Phase Simulation. The discrete phase model (DPM) was used to predict particle transport behavior in the air, which was essentially the simulation of continuous gas phase and dispersed particle two-phase flow in the air. This model used one-way coupling to calculate particle transport and was widely used to simulate particle dispersion in the air [38]. Firstly, the stable flow field is calculated, then introduced the discrete particle phase, tracked, and drew its motion trajectory. At the same time, the discrete random walk model was applied to simulate the dispersion of particles due to turbulence [29, 39]. Smoke particles were simulated as spherical particles with a density of $1 \times 10^{12}\,\mu g/m^3$, a diameter of

0.3 microns, and a mass velocity of $3.5325 \times 10^{-5}\,\mu g/s$. The mass velocity was converted from the experimental measurements. The data measured by the TSI 3330 optical particle size analyser showed that more than 70% of the smoke particles had a particle size of approximately 0.3 microns, as shown in Figure 4. Notably, electrosurgical instruments can produce particles as small as 0.3 microns [3, 4, 40]. Therefore, the particle size in the simulation was set to 0.3 microns. In this study, the steady-state flow field of the three ventilation patterns was first calculated, and the transient calculation was then conducted by setting the particle phase. The unsteady state simulation calculation is 900 s in total, with particle release for the first 600 s. In order to ensure a stable state, we performed a comparative calculation of releasing 2000 particles, 2500 particles, and 3000 particles per second. Results show that the number of particle tracks of 2000×600 cannot reach the statistical result of convergence. The statistical effect of convergence can be achieved when 2,500 particles and 3,000 particles are released per second. Finally, we chose to release 2500 particles per second for subsequent research. It is closer to the experimental data and the particles can fill the room well. At the same time, the particle trace number of 2500×600 is enough to achieve the statistical result of convergence. The time step is set to 1 s to fully track the movement path of smoke particles.

$$\frac{\partial u_p}{\partial t} = F_D(u - u_p) + \frac{g(\rho_p - \rho)}{\rho_p} + F_x,$$

(2)

where u_p is the particle velocity; u is the air velocity; $F_D(u - u_p)$ is the resistance per particle mass; ρ_p and ρ are the densities of the particles and air, respectively; F_x is the additional force; and g is the gravitational acceleration vector.

In calculating the motion of particles, additional forces depend on the properties of airflow and particles. The pressure gradient, Basset, and virtual mass forces were ignored because of the small ratio of air density to particle density [41, 42]. In this study, the Stokes-Cunningham drag law was applied to calculate the drag force. The additional forces included the Brownian, Saffman, and thermophoretic forces. We assumed that the particles have left the area when they reached the vent; therefore, we set the vent to the escape condition. Moreover, when particles encounter hard surfaces and walls, they generally do not possess enough rebound energy to resist adhesion; therefore, the surfaces and walls in the operating room are set as trap conditions. Owing to the constant temperature and humidity in the operating room, there was no significant difference in the temperature of the return air; therefore, the influence of the environmental temperature difference on airflow and particulate matter was ignored.

To compare the pollutant distribution in different regions, we introduce the local relative pollutant exposure index (e_p^c) [43]. This value was also used in similar studies and is defined as

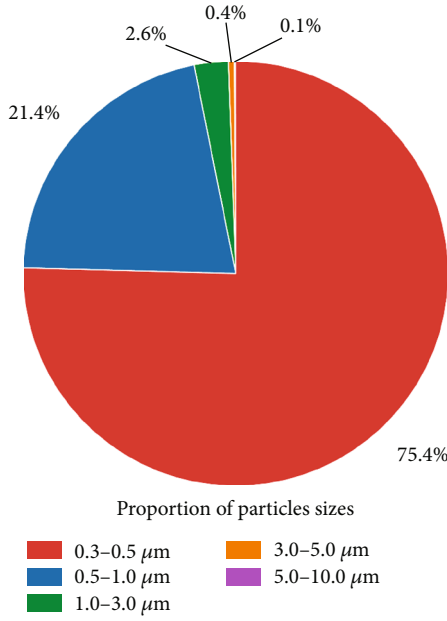$$e_p^c = \frac{c_i - c_s}{c_e - c_s},$$

(3)

FIGURE 4: Size distribution of the particles.

where c_i is the average concentration of particulate matter at a certain point in the operating room, c_e is the average concentration of particulate matter at the exhaust port, and c_s is the concentration of particulate matter in the intake air. When c_i is the indoor average concentration, e_p^c is the spatial relative pollutant exposure index.

3.3. Numerical Model Grid Independence.

The integrated computer-aided engineering and manufacturing (ICEM) computational fluid dynamics (CFD) ANSYS software was used to divide the physical model through structured grids of different sizes, and three types of grids, namely, 2569882, 3552736, and 5098912, were obtained. For the three different meshes, mesh sizes of 4, 2, and 2 cm were set for the surgical staff surfaces. The mesh sizes of the supply diffuser and exhaust were 5 cm. The mesh sizes at the surface of the equipment were 4, 2, and 2 cm. The global sizes were 12, 10, and 8 cm, respectively. The grid independence was verified by measuring the air velocities at points on two lines near the rear end of the operating table. The results are shown in Figure 5. The variation trends of the three grid speeds were consistent, and the difference was small, indicating that the independence of the grid was acceptable. Additionally, the sensitivity of the mesh size was tested by comparing the simulation results for different mesh numbers. The grid convergence index (GCI) [44] was calculated using Equation (4) to evaluate the quality of the selected grid. The results showed that all the GCI values were less than 6.2% for the selected mesh sizes, indicating that the mesh was adequate. Considering the complexity and accuracy of subsequent calculations, grid 3552736 was selected for subsequent calculations.

$$GCI = F_s \left| \frac{r^{acc}\delta}{1 - r^{acc}} \right| \qquad (4)$$

where $r = 2^{1/3}$ is the linear grid refinement factor, acc = 2 is the formal order of accuracy (second-order), and $F_s = 1.25$ is the safety factor, as suggested by previous studies [44, 45], and δ is the difference of the variables between the described mesh and a refined mesh.

4. Results and Discussion

4.1. Numerical Model Validation. The airflow field in the simulation was verified to ensure the accuracy of numerical calculations. Figure 3 shows the positions of the six guides at the two heights. Figure 6 shows a comparison between the simulated velocity values at each point of the six lines and those at the experimental measurement points. The results showed that the simulated values were consistent with the experimental values. Owing to the error of the anemometer in the experiment and the simplification of the model in the numerical simulation, the difference between the experimental and simulated values was reasonable, and the simulation results were acceptable.

The simulation and experimental values of the smoke particle concentration were verified, and the results are shown in Figure 7. For the experimental data, we averaged the values of three repeated experiments at each sampling point at the determined time, subsequently averaged the values obtained at three sampling points, and standardised the concentration value at each sampling point with this value. The error value was then obtained by calculating the standard deviation. To process the simulation values, the smoke particle concentrations at the three sampling points at the determined time were averaged, and the simulated concentration values at each sampling point were standardised using this value. Although the experimental result is not completely consistent with the simulated value, considering the complexity of the experimental conditions and the error of the measuring instrument, the deviation does not affect the overall trend of smoke particle concentration at different sampling points at different times. Therefore, the result is acceptable, and the accuracy of the subsequent simulation can be guaranteed.

4.2. Spatial and Temporal Distribution of Airflow Field and Particles. At the designed air volume, the airflow fields of the three ventilation patterns and the particle positions at different times are shown in Figure 8. Figure 8(a) shows the velocity vector diagram, flow diagram, and the diffusion of smoke particles of $X = 0$ and $Y = 0$ sections in the operating room under the VLAF system. The flow from the diffuser in the centre of the ceiling was accelerated by gravity and flowed vertically downward through the operating area. However, the high-speed airflow was forced to change direction as it was obstructed by the operating lamp, forming eddy currents under the operating lamp and resulting in no vertical airflow in front of the attending physician and assistant. As air flows over the staff and patients, it slows down near the body because of the body's heat plume. Part of the airflow is deflected to both sides at a large angle after encountering the operating table, and a small part of the airflow forms a small eddy current under the operating table.
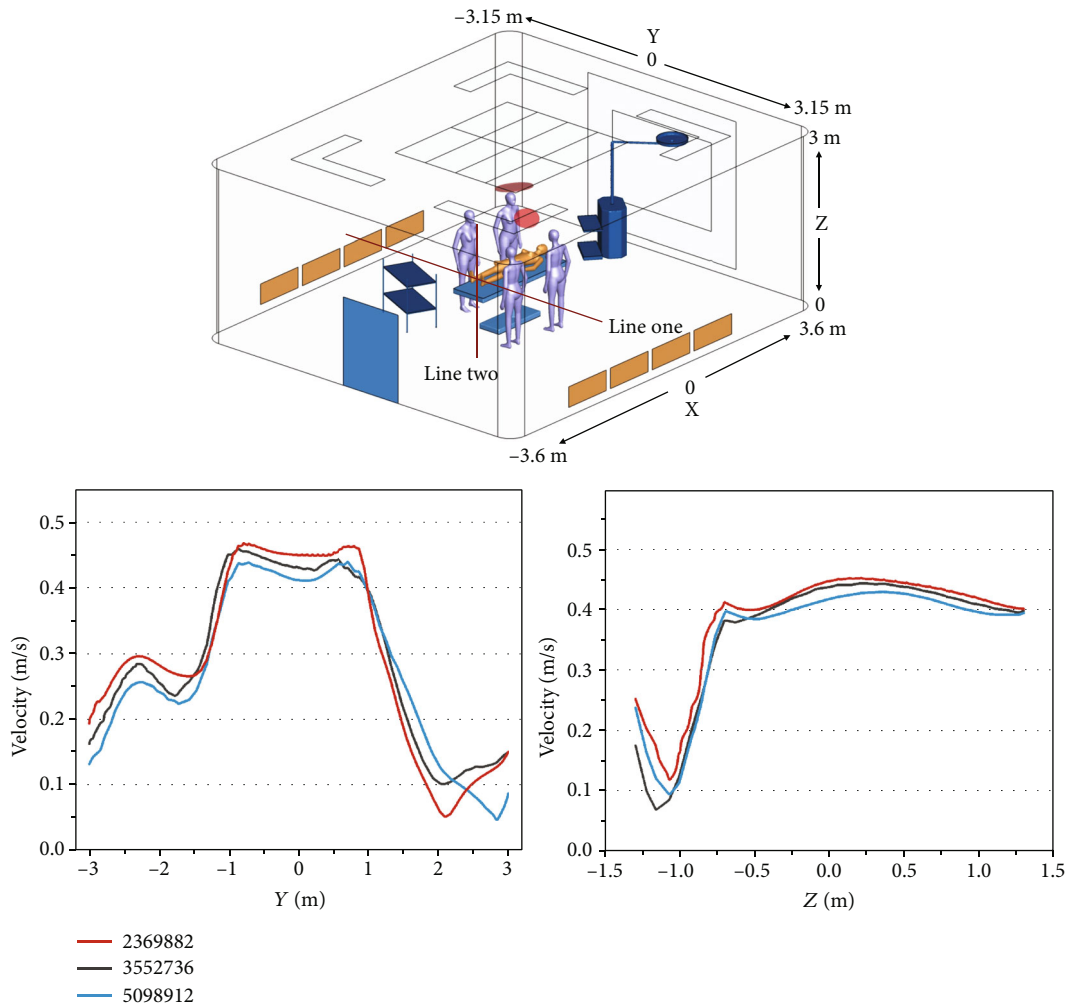
FIGURE 5: Grid independence verification reference line position diagram and speed comparison between three grid numbers.

When the diffused air hits the wall, it begins to move upward and forms a large eddy outside the surgical area with a lower velocity at its centre. As for the smoke particles, as the airflow is blocked by the operating lamp and its own thermal buoyancy, the smoke particles first move to the top of the patient's head after generation, and most of the particles then quickly move down to the $X+$ and $Y-$ corners under the influence of the vertical airflow. At this point, a small number of particles remained in the vortex region in the corner, and most of the particles changed direction and moved up the wall. When the particles reached the ceiling, they began to move diagonally downward and gradually diffused.

The airflow and particulate matter in the operating room equipped with the HLAF ventilation system are shown in Figure 8(b). The airflow begins from a wall diffuser on one side and blows horizontally across the surgical area. The airflow over the operating lamp is blocked, changing direction and forming a low-speed eddy zone behind the operating lamp. After the airflow reaches the wall through the surgical area, it is blocked from flowing into the ground. Finally, it rises near the surgical area, forming a large eddy current in the space. The airflow distribution on both sides of the operation area was chaotic. Except for some airflow to the

exhaust port, most of the airflow was towards the roof and formed a low-speed vortex near the corner. Immediately, after the smoke is produced, it follows the horizontal airflow towards the leg of the patient. Subsequently, a large amount of deposition occurred along the direction of the vortex moving towards the wall. Simultaneously, some particles returned to the space with the airflow and gradually diffused.

The airflow and particulate matter in the operating room equipped with the UDAF + mixing ventilation system are shown in Figure 8(c). In this system, the airflow pattern in the operation area is similar to that of VLAF ventilation, but the vortex under the operating table is significant, which may be ascribed to the interference of the airflow outside the operation area. Moreover, external airflow affects the vertical airflow in the surgical area, forcing it to change its direction in advance. However, a relatively high-velocity horizontal airflow formed near the patient, which ensured the removal of smoke particles in the surgical area. Compared to that of traditional VLAF ventilation, the space outside the surgical area in the UDAF + mixing system produces a larger eddy area with a smaller but more stable airflow velocity. Owing to the obstruction of the operating lamp, the smoke particles first rose upward under the action of thermal buoyancy, and
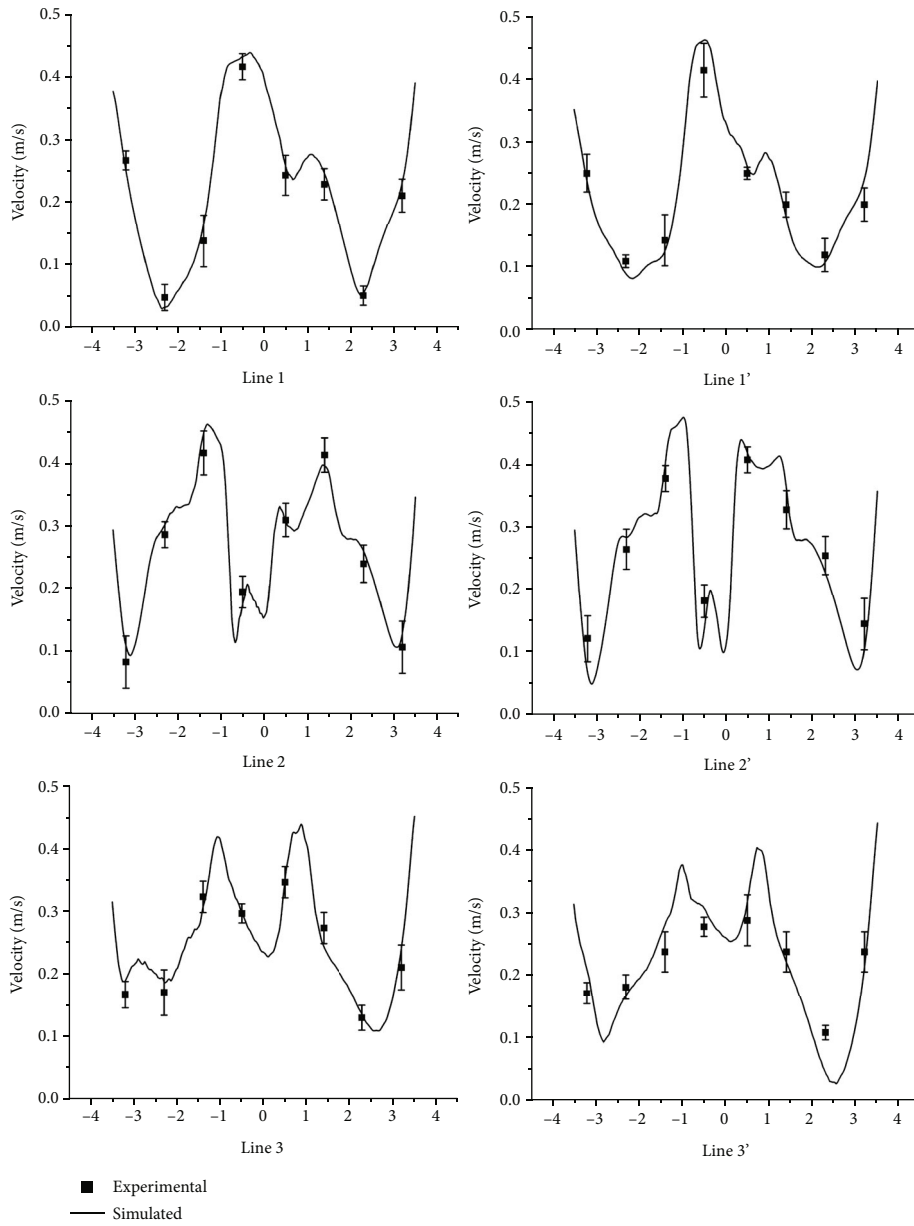
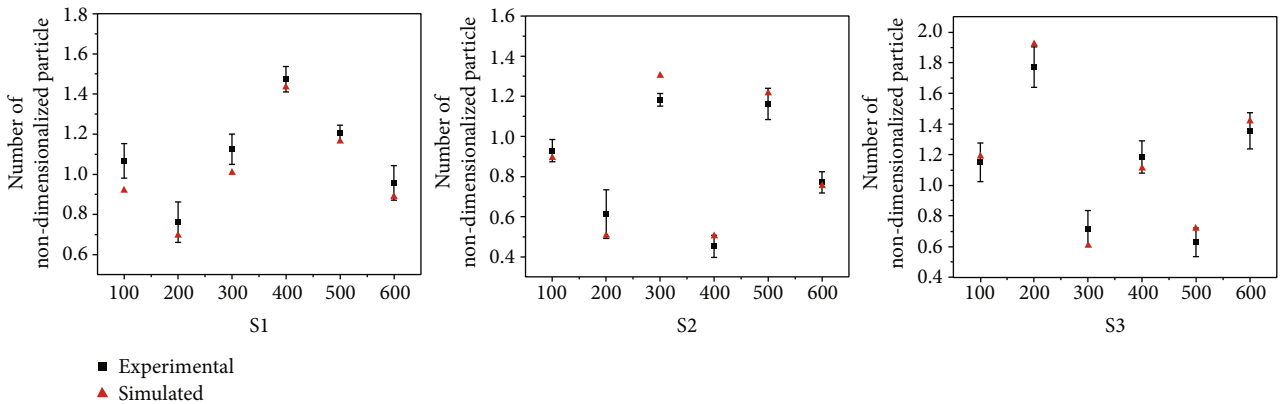FIGURE 6: Comparison of simulated and experimental wind speed results.

FIGURE 7: Comparison of the number of dimensionless particles in experimental and simulated results.
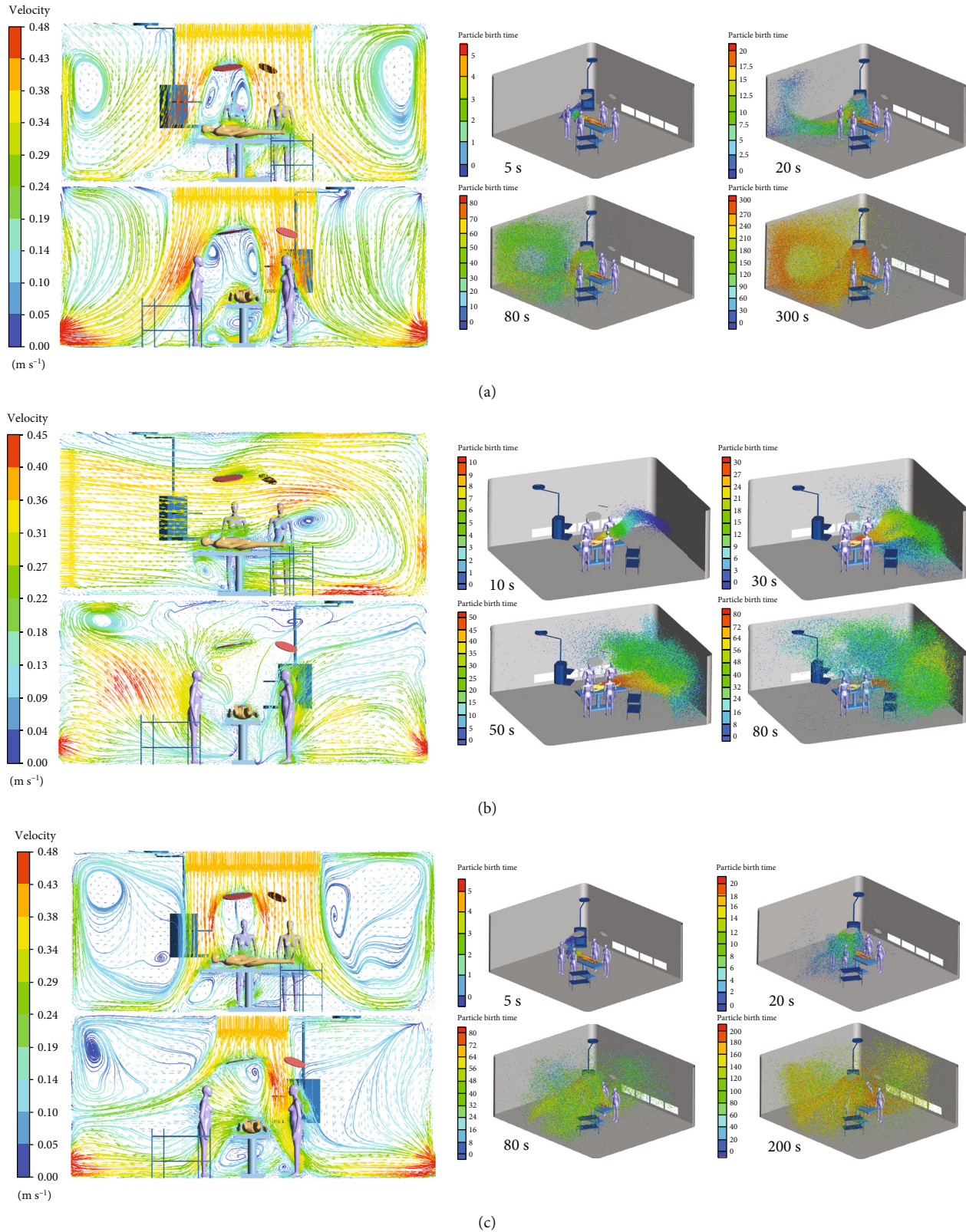
FIGURE 8: Airflow and particle conditions in the operating room under three types of ventilation. (a) VLAF; (b) HLAF; (c) UDAF + mixing.

some of the particles remained in the eddy current near the operating lamp. With an increase in the number of particles, most particles moved towards the exhaust vents on both

sides with the vertical airflow. However, owing to the obstruction from medical staff and equipment along the way, the direction of movement of the particles was
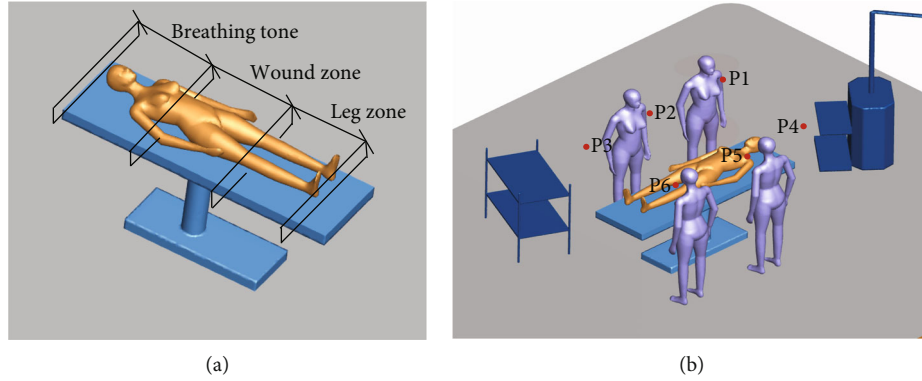
(a)

(b)

FIGURE 9: (a) Division of the area around the patient. (b) Particle detection site near medical staff.

deflected, and some particles diffused into space or were trapped in the eddy current area.

4.3. Distribution of Smoke Particles in the Operating Area. Additionally, a cube with dimensions of $2.4 \times 2 \times 1\,m$ ($X \times Y \times Z$) was constructed in the entire area with the medical staff and patients, from the patient to the head of the medical staff, representing the working area. In the physical model, the length, width, and height coordinate ranges of this region are $X = -1.2$ to $1.2\,m$, $Y = -1$ to $1\,m$, and $Z = 0.8$ to $1.8\,m$, respectively.

To further study the concentration distribution of particulate matter in the surgical area, we selected three areas on the upper side of the patient and six points in front of the medical staff (Figure 9). The six points were located on the same plane, near the mouth and nose of the medical workers, to monitor changes in the particle concentration in their respiratory areas. The four points P1, P2, P5, and P6 were located 0.2 m in front of the faces of the medical staff, and the distance between the two points on each side was 0.9 m. We used five different ACH values (40, 50, 60, 70, and 80) to study and evaluate the three different ventilation patterns.

Figure 10(a) shows that in the operating room equipped with the VLAF ventilation system, the area with the highest local relative pollutant exposure index near the patient was always located in the patient's respiratory area, wherein the highest exposure index reached 15.73. This may be attributed to the obstruction by the operating lamp, which causes the accumulation of smoke particles in the patient's breathing area. With an increase in the ACH value, the e_p^c of each region changes significantly. When the ACH value was less than 60, the e_p^c in each region increased with increasing ACH. The e_p^c of each region decreased rapidly after the ACH value exceeded 60. The indoor relative pollutant exposure coefficient reached the lowest value of 0.68 when the ACH was 70. Beyond an ACH value of 70, e_p^c did not decrease significantly. This may be because the vertical downward laminar airflow is blocked by obstacles midway, such as the surgical lamp and medical staff. This destroys the clearance effect of vertical airflow on particulate matter and generates many

small vortices near the obstacles, thereby hindering the removal of accumulated particulate matter.

In the vicinity of the medical staff, as shown in Figure 10(b), the concentration at point P1 near the assistant's face showed the most obvious range of change accompanied by a change in the ACH value and was much higher than that at the other points. When $T = 600\,s$, the highest and lowest concentrations at P1 were 1.55×10^{-3} and $5.12 \times 10^{-4}\,\mu g/m^3$ when the ACH values were 50 and 70, respectively. When the time reached 720 s (the end of surgery was after 120 s), the concentration at each point decreased to less than $1.5 \times 10^{-5}\,ug/m^3$; at this time, if the ACH is more than 60, the concentration at each point can be lower than $3 \times 10^{-6}\,\mu g/m^3$. Notably, the particle concentration at point P2 near the attending doctor was the highest at this time, which may be because the airflow here was affected by the operating lamp, resulting in an eddy current, which led to the retention of particles that were difficult to eliminate.

Figure 11(a) shows that in the operating room equipped with a HLAF ventilation system, when the ACH value is less than 60, HLAF cannot remove smoke particles in the operating area, and the e_p^c near the patient was up to 28.26. After more than 60 breaths, the horizontal airflow carries particles from the patient's respiratory and wound areas to the patient's legs. At this point, the maximum e_p^c value in the leg zone was 12.27. When the ACH value increased to 70, the HLAF system had a washing effect on the entire surgical area; however, at this time, relatively high concentrations of particulate matter were observed in the leg and wound areas of the patient. There may be two reasons for the above: one is due to obstruction of laminar airflow by the patient and surgical lights that can generate the small changes and small eddy currents in the vicinity of a patient's body resulting in particulate retention; the other is that the airflow hitting the wall forms a large vortex in the space, which affects the leg area of the patient.

In the vicinity of the medical staff, as shown in Figure 11(b), when the ACH value is less than 70, the particulate matter concentrations at P4, P5, and P6 are very high in the first 200 s due to the obstruction of horizontal airflow by the medical equipment. The smoke particles moved in the operating room with the air currents. At 200 s, particulate
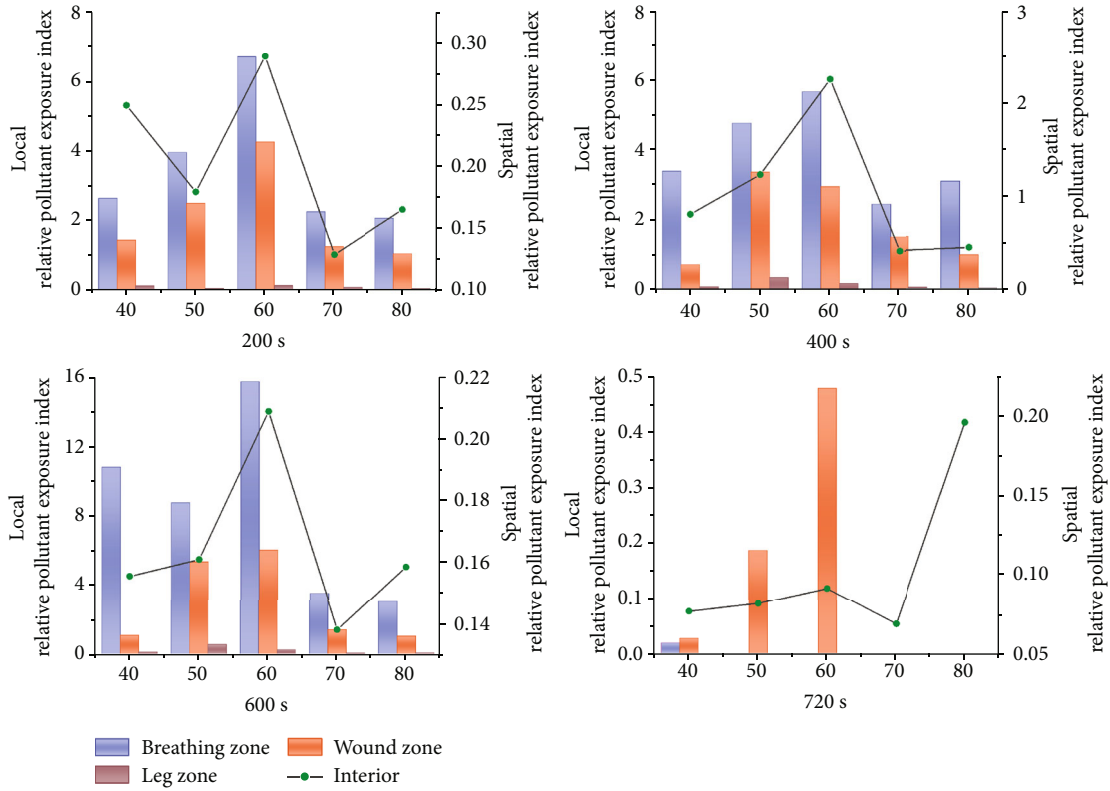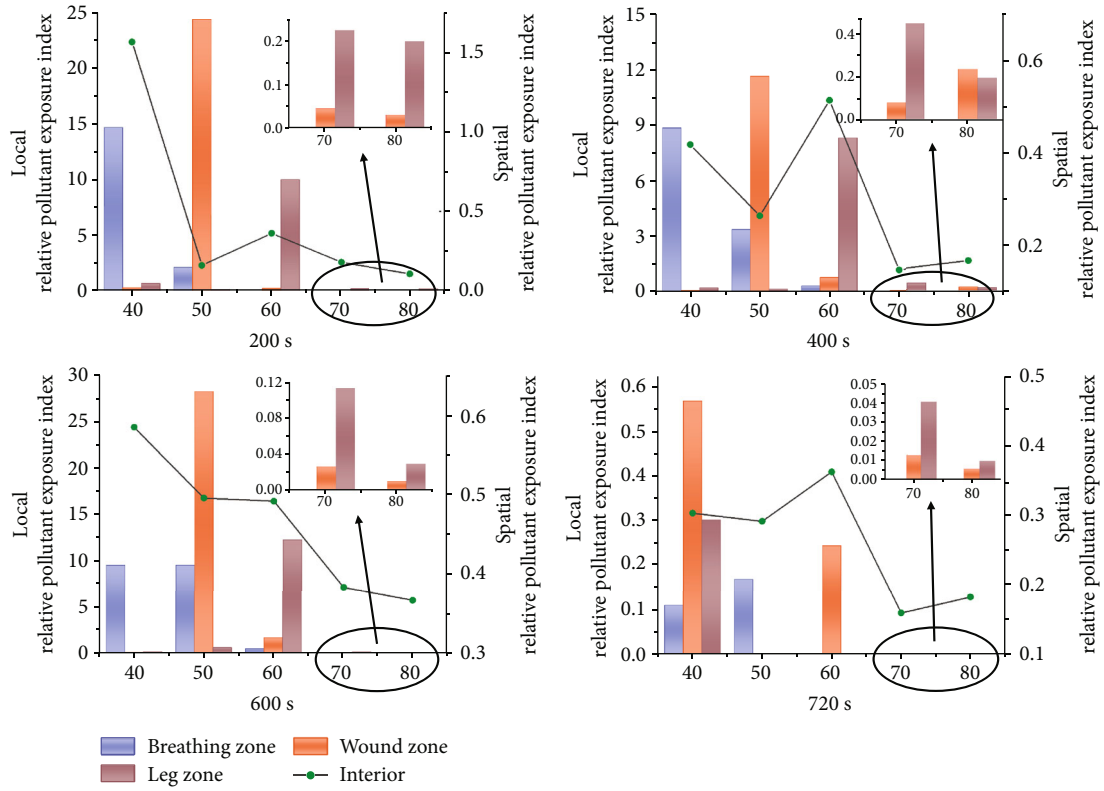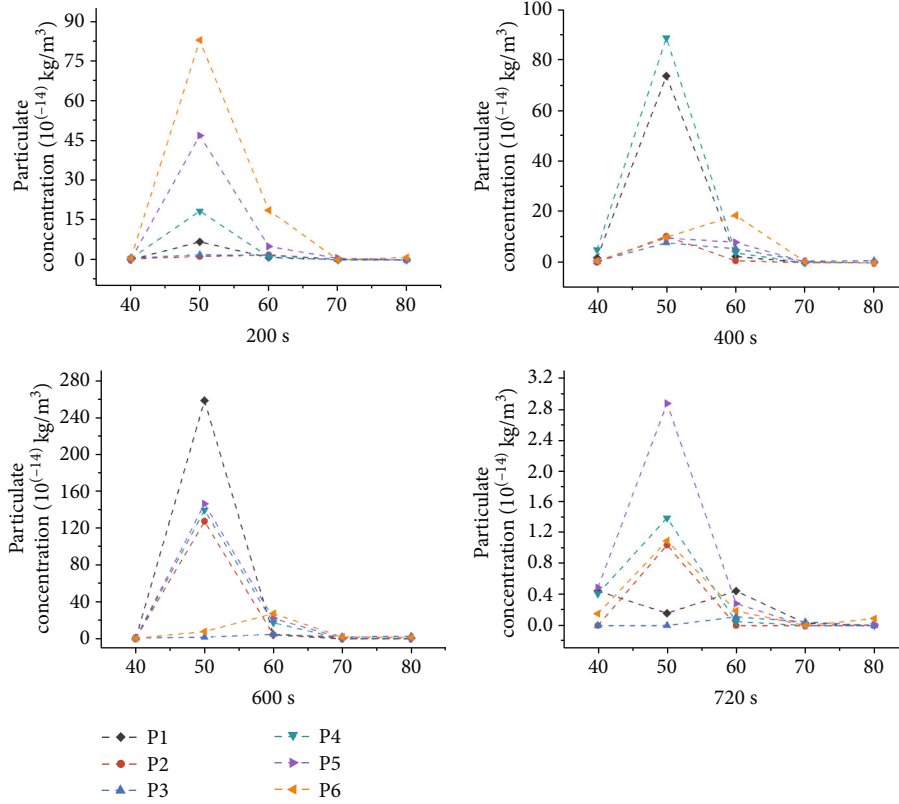
(a)
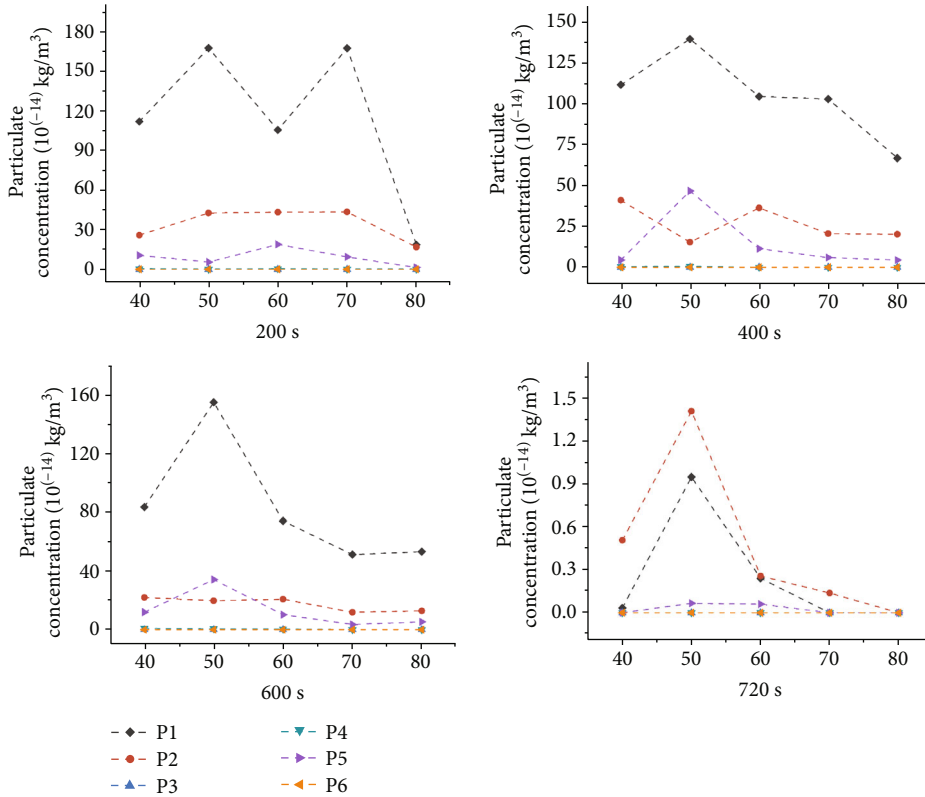
(b)

FIGURE 10: Distribution of smoke particles at different ACH under VLAF (a) near the patient and (b) near the medical staff.
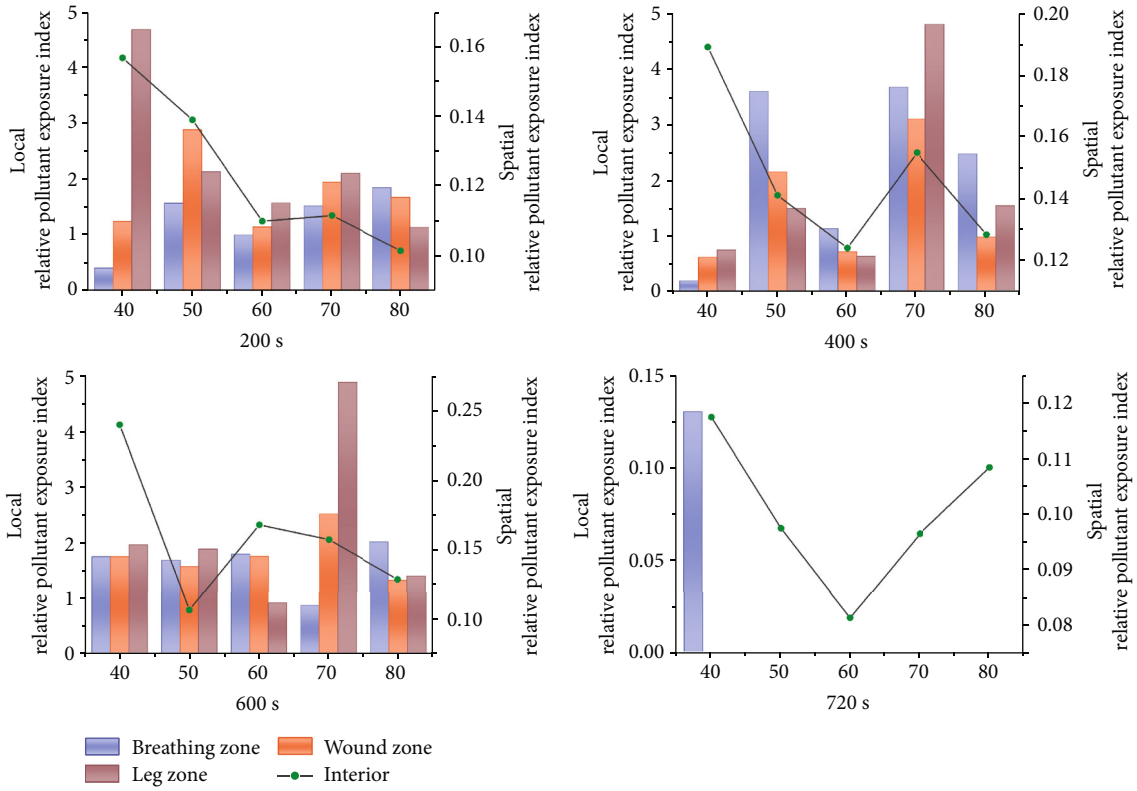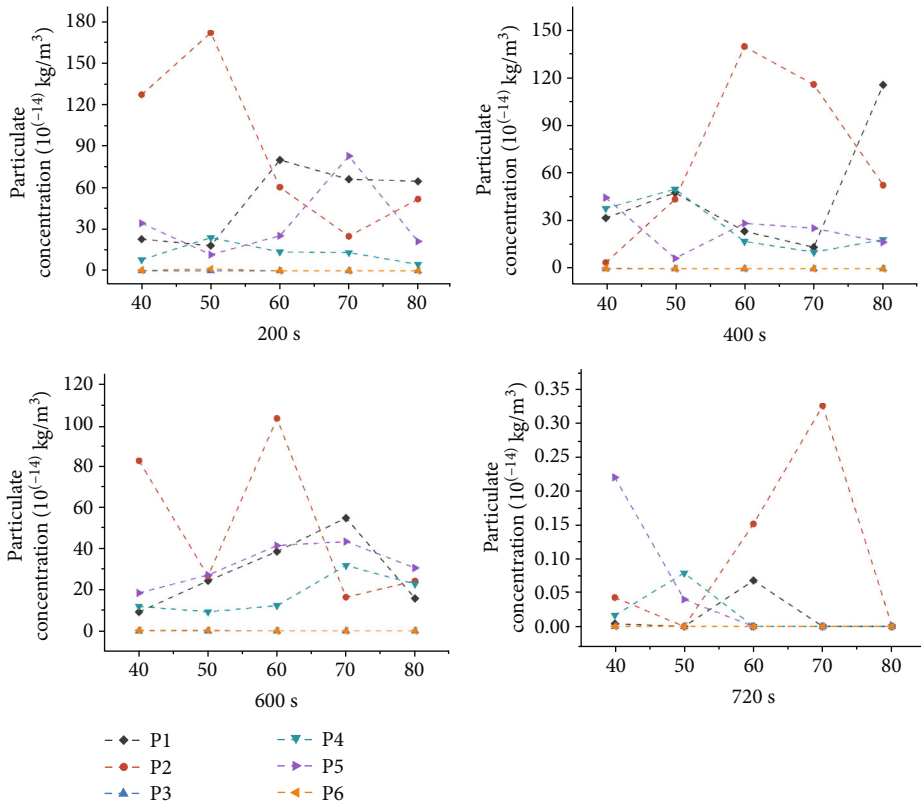
(a)

(b)

Figure 11: Distribution of smoke particles at different ACH under HLAF (a) near the patient and (b) near the medical staff.

(a)

(b)

FIGURE 12: Distribution of smoke particles at different ACH under UDAF + mixing (a) near the patient and (b) near the medical staff.

matter accumulated in large quantities at point P2 near the wound, resulting in a relatively high concentration. Driven by the horizontal airflow, particulate matter continuously moves towards the patient's legs, resulting in an increasing concentration at point P4. Over time, more particles hit the wall with airflow and spread through the room, gathering near the assistant. Thus, at 600 s, the concentration at P1 is relatively high. At 720 s, most of the particles were discharged from the air with the airflow, but near P5, the obstruction of airflow by the equipment resulted in the accumulation of a large number of particles, which was difficult to remove. Therefore, the concentration of the particles at this point was relatively high.

As shown in Figure 12(a), compared to that with the other two systems, the operating room equipped with the UDAF + mixing system has little difference in e_p^c in each area, and is less affected by the ACH, and the overall particulate matter level is more stable. This may be due to the reduced area of the vertical laminar air supply, more significant obstruction of the vertical airflow by the operating lamp, and the eddy current generated above the patient's thermal plume, resulting in a uniform particle distribution. Compared to those in the other two conditions, the e_p^c of each area above the patient in the UDAF + mixing system was below 5, the indoor relative pollutant exposure coefficient was always below 0.2, and the overall stability was at a lower level without a high peak. All the e_p^c values were less than 1 when the ACH value was 60 and 400 s. This may be ascribed to the fact that the airflow provided by the surrounding air supply outlet not only dilutes the particle concentration in the surrounding area but also strengthens the airflow to the exhaust port and enhances the exclusion effect of particles in the surgical area and room. This is also observed in the e_p^c values of each region after 720 s; at this time, the e_p^c values of the region above the patient in the operating room equipped with the UDAF + mixing system basically tend to 0, lower than those of the other two conditions.

Figure 12(b) shows the respiratory surface of medical staff. The concentrations at P3 and P6 are always close to 0, and those at other points change significantly with changes in the ACH value; however, the concentrations at all the points are in a low range. When $T = 600$ s, the concentrations at point P2 near the attending doctor reached the highest and lowest values of 9.2×10^{-4} and 1.6×10^{-4} $\mu g/m^3$ when the ACH values were 60 and 70, respectively. The remaining points showed a tendency to increase with the ACH. This may be because the airflow provided by the surrounding air supply port enhances the airflow to the exhaust port, which improves the removal effect of indoor particulate matter. Airflow carries more particles through medical staff, resulting in a large amount of particulate matter diffusion and retention. When the time reached 720 s, the particle concentration at all points in the operation area, except P2, decreased to 1×10^{-6} $\mu g/m^3$, which is lower than that of the other two ventilation patterns, indicating that the UDAF + mixing system is more effective in removing particulates in the operation area. At this time, the concentration at point P2 near the attending doctor is relatively high, which may be caused by the blocking effect of
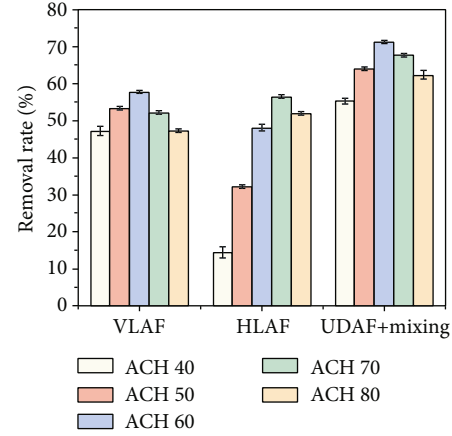

FIGURE 13: Removal rate of smoke particles in operating room under different ventilation systems.

the surgical lamp on the vertical airflow, similar to that in the VLAF system.

In the VLAF system, the particulate matter concentration in the patient's respiratory and wound areas should be noted during surgery, and local smoke exhaust devices should be strengthened in this area. The attending physician and assistant should pay attention to the effectiveness of protective measures to avoid harm caused by smoke particles. For the HLAF system, an adequate air volume should first be ensured in the operating room, followed by smoke removal measures below the patient's wound. Medical staff near the patient's leg should strengthen the protective measures. The peripheral areas on both sides of the exhaust vent have chaotic flow, and the residence time of particles is long; therefore, medical staff should avoid staying there for long periods. The UDAF + mixing system in the operating room had a low overall concentration distribution in the operating area during operation. The main focus should be on the protection from smoke particles at the wound site, and the medical staff on the path from the wound to the exhaust outlet should pay special attention to these particles. The HLAF system is effective in removing smoke particles in the surgical area when a sufficient air volume is maintained. The UDAF + mixing system is the most stable in the surgical area compared to the other two systems, which maintains the concentration in the area at a lower range and is more effective in removing smoke particles.

4.4. Removal Efficiency of Smoke Particles under Different Ventilation Patterns.

Figure 13 shows the removal rate of the operating room under the three ventilation patterns and different ACH values. The removal rate here was defined as the ratio of the total emission of particulate matter in the operating room to the total production at the end of the operation [46]. Notably, large ACH values do not represent a better removal effect. The VLAF and UDAF + mixing systems had the highest removal rates of 58.76% and 71.39%, respectively, at an ACH value of 60. When the ACH value was 70, the removal rate of the HLAF system was the best,

with a value of 61.54%. The UDAF + mixing system had a better removal efficiency than the other two systems.

5. Conclusions

In this study, experiments and CFD simulations were used to explore the spatial concentration distribution and variation of smoke particles under VLAF, HLAF, and UDAF + mixing ventilation systems in an operating room. The main conclusions are as follows:

(1) For the VLAF system, the concentration of smoke particles in the operating area was high because of the blockage of the operating lights. Increasing the ACH did not significantly reduce the concentration of smoke particles. The HLAF system was significantly affected by the ACH, and once the ACH was below 70, the indoor air cleanliness deteriorated significantly

(2) The UDAF + mixing system was a more effective ventilation pattern, and the optimal ACH value was approximately 60. At this time, the local pollutant exposure index near patients in the operating room was very small, the particle concentration near the medical staff was less than $9 \times 10^{-4}\ \mu g/m^3$, and the particle concentration in the operating area was stable at a low level

(3) Increasing the ACH did not achieve a better removal effect. Compared to that in the other two cases, the airflow distribution of the UDAF + mixing system was more conducive to particle removal, and the highest removal rate was 71.39%. However, in this case, the medical staff on the path from the wound to the exhaust outlet should ensure protection from particles

Considering these results, this study shows that the UDAF + mixing system is an alternative to laminar ventilation systems. The system can stably control the concentration of smoke particles in the operating area within a low range while ensuring a high indoor particle removal efficiency. Moreover, the layout of the operating room equipment and airflow distribution has a significant influence on the distribution and removal of particles. A study on the optimal equipment layout scheme and airflow distribution optimisation for each ventilation pattern will be conducted in future studies.

Data Availability

The data that support the findings of this study are available from the corresponding author upon reasonable request.

Additional Points

Practical Implications. (i) Surgery smoke particle concentration is not to be ignored, and ventilation pattern, air change rate, and indoor layout seriously affect the indoor clean environment. (ii) The migration, distribution, and removal of smoke particle in the operating room under different ventilation patterns were quantitatively analysed, and the high concentration area was determined. The research results effectively support the prevention and control of smoke particles. (iii) Central unidirectional airflow and peripheral mixing are effective ventilation.

Conflicts of Interest

The authors declare that they have no known competing financial interests or personal relationships that could have appeared to influence the work reported in this paper.

Authors' Contributions

Zhijian Liu conducted the conceptualization, methodology, funding acquisition, supervision, project administration, and writing of the review and editing. Zheng Zhang conducted the methodology, software, validation, formal analysis, data curation, and writing of the original draft. Jiabin Lv conducted the project administration, resources, and writing of the review and editing. Juntao Ma managed the software and investigation. Guangpeng Yao conducted the writing of the review and editing, software, and formal analysis. Junzhou He conducted the writing of the review and editing. Guoqing Cao managed the resources and supervision.

Acknowledgments

References

[1] C. He, I. M. Mackay, K. Ramsay et al., "Particle and bioaerosol characteristics in a paediatric intensive care unit," *Environment International*, vol. 107, pp. 89–99, 2017.

[2] G. Buonanno, R. Capuano, G. Cortellessa, and L. Stabile, "Airborne particle emission rates and doses received in operating rooms from surgical smoke," *Building and Environment*, vol. 151, pp. 168–174, 2019.

[3] F. Romano, S. Milani, J. Gustén, and C. M. Joppolo, "Surgical smoke and airborne microbial contamination in operating theatres: influence of ventilation and surgical phases," *International Journal of Environmental Research and Public Health*, vol. 17, no. 15, p. 5395, 2020.

[4] F. Romano, J. Gustén, S. De Antonellis, and C. Joppolo, "Electrosurgical smoke: ultrafine particle measurements and work environment quality in different operating theatres," *International Journal of Environmental Research and Public Health*, vol. 14, no. 2, p. 137, 2017.

[5] K. Ishihama, S. Sumioka, K. Sakurada, and M. Kogo, "Floating aerial blood mists in the operating room," *Journal of Hazardous Materials*, vol. 181, no. 1-3, pp. 1179–1181, 2010.

[6] R. Karuppal, S. Surendran, G. Patinharayil, V. V. Muhammed Fazil, and A. Marthya, "It is time for a more cautious approach to surgical diathermy, especially in COVID-19 outbreak: a schematic review," *Journal of Orthopaedics*, vol. 20, pp. 297–300, 2020.

[7] Y. Li, "Hypothesis: SARS-CoV-2 transmission is predominated by the short-range airborne route and exacerbated by poor ventilation," *Indoor Air*, vol. 31, 925 pages, 2021.

[8] E. Alp, D. Bijl, R. P. Bleichrodt, B. Hansson, and A. Voss, "Surgical smoke and infection control," *Journal of Hospital Infection*, vol. 62, no. 1, pp. 1–5, 2006.

[9] H. H. Najafabadi, V. Suresh, C. J. Thomas Spence, E.-L. Teh, and J. E. Cater, "Development of a numerical model of surgical smoke during laparoscopy," *International Journal of Heat and Mass Transfer*, vol. 175, article 121253, 2021.

[10] B. Ulmer, "Occupational Safety and Health Administration acts on guidelines for electrosurgical smoke," *AORN Journal*, vol. 67, no. 6, pp. 1244-1245, 1998.

[11] P.-C. Cheng, M.-H. Wen, W.-L. Hsu, P.-W. Cheng, and L.-J. Liao, "A study to quantify surgical plume and survey the efficiency of different local exhaust ventilations," *Scientific Reports*, vol. 11, no. 1, p. 14096, 2021.

[12] S. Scaltriti, S. Cencetti, S. Rovesti, I. Marchesi, A. Bargellini, and P. Borella, "Risk factors for particulate and microbial contamination of air in operating theatres," *Journal of Hospital Infection*, vol. 66, no. 4, pp. 320–326, 2007.

[13] J. Park, S. Y. Yoo, J.-H. Ko et al., "Infection prevention measures for surgical procedures during a Middle East respiratory syndrome outbreak in a tertiary Care hospital in South Korea," *Scientific Reports*, vol. 10, no. 1, p. 325, 2020.

[14] A. L. Steege, J. M. Boiano, and M. H. Sweeney, "Secondhand smoke in the operating room? Precautionary practices lacking for surgical smoke," *American Journal of Industrial Medicine*, vol. 59, no. 11, pp. 1020–1031, 2016.

[15] D. Hansen, C. Krabs, D. Benner, A. Brauksiepe, and W. Popp, "Laminar air flow provides high air quality in the operating field even during real operating conditions, but personal protection seems to be necessary in operations with tissue combustion," *International Journal of Hygiene and Environmental Health*, vol. 208, no. 6, pp. 455–460, 2005.

[16] J. M. Boyce and D. Pittet, "Guideline for hand hygiene in health-care settings: recommendations of the Healthcare Infection Control Practices Advisory Committee and the HIC-PAC/SHEA/APIC/IDSA Hand Hygiene Task Force," *Infection Control and Hospital Epidemiology*, vol. 23, 12 Suppl, pp. S3–S40, 2002.

[17] M. Woloszyn, J. Virgone, and S. Mélen, "Diagonal air-distribution system for operating rooms: experiment and modeling," *Building and Environment*, vol. 39, no. 10, pp. 1171–1178, 2004.

[18] Y. Li, P. Cheng, and W. Jia, "Poor ventilation worsens short-range airborne transmission of respiratory infection," *Indoor Air*, vol. 32, no. 1, Article ID e12946, 2022.

[19] S. Wong, H. Chen, D. C. Lung, P. Ho, K. Yuen, and V. C. Cheng, "To prevent SARS-CoV-2 transmission in designated quarantine hotel for travelers: is the ventilation system a concern?," *Indoor Air*, vol. 31, 1297 pages, 2021.

[20] C. Wang, S. Holmberg, and S. Sadrizadeh, "Numerical study of temperature-controlled airflow in comparison with turbulent mixing and laminar airflow for operating room ventilation," *Building and Environment*, vol. 144, pp. 45–56, 2018.

[21] M. Diab-Elschahawi, J. Berger, A. Blacky et al., "Impact of different-sized laminar air flow versus no laminar air flow on bacterial counts in the operating room during orthopedic surgery," *American Journal of Infection Control*, vol. 39, no. 7, pp. e25–e29, 2011.

[22] T. Hirsch, H. Hubert, S. Fischer et al., "Bacterial burden in the operating room: impact of airflow systems," *American Journal of Infection Control*, vol. 40, no. 7, pp. e228–e232, 2012.

[23] T. T. Chow and X. Y. Yang, "Ventilation performance in the operating theatre against airborne infection: numerical study on an ultra-clean system," *The Journal of Hospital Infection*, vol. 59, no. 2, pp. 138–147, 2005.

[24] C. Méndez, J. F. San José, J. M. Villafruela, and F. Castro, "Optimization of a hospital room by means of CFD for more efficient ventilation," *Energy and Buildings*, vol. 40, no. 5, pp. 849–854, 2008.

[25] W. A. C. Zoon, M. G. M. van der Heijden, M. G. L. C. Loomans, and J. L. M. Hensen, "On the applicability of the laminar flow index when selecting surgical lighting," *Building and Environment*, vol. 45, no. 9, pp. 1976–1983, 2010.

[26] T.-T. Chow and X.-Y. Yang, "Performance of ventilation system in a non-standard operating room," *Building and Environment*, vol. 38, no. 12, pp. 1401–1411, 2003.

[27] J. Liu, H. Wang, and W. Wen, "Numerical simulation on a horizontal airflow for airborne particles control in hospital operating room," *Building and Environment*, vol. 44, no. 11, pp. 2284–2289, 2009.

[28] B. Zhao and J. Wu, "Numerical investigation of particle diffusion in a clean room," *Indoor and Built Environment*, vol. 14, no. 6, pp. 469–479, 2005.

[29] S. Sadrizadeh, A. Tammelin, P. Ekolind, and S. Holmberg, "Influence of staff number and internal constellation on surgical site infection in an operating room," *Particuology*, vol. 13, pp. 42–51, 2014.

[30] B. Zhao, X. Li, and Z. Zhang, "Numerical study of particle deposition in two differently ventilated rooms," *Indoor and Built Environment*, vol. 13, no. 6, pp. 443–451, 2004.

[31] F. Romano, L. Marocco, J. Gustén, and C. M. Joppolo, "Numerical and experimental analysis of airborne particles control in an operating theater," *Building and Environment*, vol. 89, pp. 369–379, 2015.

[32] S. H. Choi, T. G. Kwon, S. K. Chung, and T.-H. Kim, "Surgical smoke may be a biohazard to surgeons performing laparoscopic surgery," *Surgical Endoscopy*, vol. 28, no. 8, pp. 2374–2380, 2014.

[33] Z. Liu, M. Zhang, G. Cao, S. Tang, H. Liu, and L. Wang, "Influence of air supply velocity and room temperature conditions on bioaerosols distribution in a class I operating room," *Building and Environment*, vol. 204, article 108116, 2021.

[34] D. S. Hill, J. K. O'Neill, R. J. Powell, and D. W. Oliver, "Surgical smoke - a health hazard in the operating theatre: a study to quantify exposure and a survey of the use of smoke extractor systems in UK plastic surgery units," *Journal of Plastic, Reconstructive & Aesthetic Surgery*, vol. 65, no. 7, pp. 911–916, 2012.

[35] E. Küçüktopcu and B. Cemek, "Evaluating the influence of turbulence models used in computational fluid dynamics for the prediction of airflows inside poultry houses," *Biosystems Engineering*, vol. 183, pp. 1–12, 2019.

[36] K. Kwon, I. Lee, G. Q. Zhang, and T. Ha, "Computational fluid dynamics analysis of the thermal distribution of animal occupied zones using the jet-drop-distance concept in a mechanically

ventilated broiler house," *Biosystems Engineering*, vol. 136, pp. 51–68, 2015.

[37] E. Bustamante, F.-J. García-Diego, S. Calvet, A. Torres, and A. Hospitaler, "Measurement and numerical simulation of air velocity in a tunnel-ventilated broiler house," *Sustainability*, vol. 7, no. 2, pp. 2066–2085, 2015.

[38] Y. Zhou and S. Ji, "Experimental and numerical study on the transport of droplet aerosols generated by occupants in a fever clinic," *Building and Environment*, vol. 187, article 107402, 2021.

[39] J. Wei and Y. Li, "Enhanced spread of expiratory droplets by turbulence in a cough jet," *Building and Environment*, vol. 93, pp. 86–96, 2015.

[40] J. Wu, H. Shen, X. Zhan, and Y. Zhu, "Study on influencing factors and control strategies of surgical smoke concentration distribution," *Aerosol and Air Quality Research*, vol. 20, no. 12, pp. 2941–2952, 2020.

[41] B. Zhao, Y. Zhang, X. Li, X. Yang, and D. Huang, "Comparison of indoor aerosol particle concentration and deposition in different ventilated rooms by numerical method," *Building and Environment*, vol. 39, no. 1, pp. 1–8, 2004.

[42] T.-J. Chang and T.-S. Hu, "Transport mechanisms of airborne particulate matters in partitioned indoor environment," *Building and Environment*, vol. 43, no. 5, pp. 886–895, 2008.

[43] F. A. Berlanga, M. R. de Adana, I. Olmedo, J. M. Villafruela, J. F. San José, and F. Castro, "Experimental evaluation of thermal comfort, ventilation performance indices and exposure to airborne contaminant in an airborne infection isolation room equipped with a displacement air distribution system," *Energy and Buildings*, vol. 158, pp. 209–221, 2018.

[44] T. van Hooff, B. Blocken, and Y. Tominaga, "On the accuracy of CFD simulations of cross-ventilation flows for a generic isolated building: comparison of RANS, LES and experiments," *Building and Environment*, vol. 114, pp. 148–165, 2017.

[45] P. J. Roache, "Quantification of uncertainty in computational fluid dynamics," *Annual Review of Fluid Mechanics*, vol. 29, no. 1, pp. 123–160, 1997.

[46] Z. Liu, H. Liu, H. Yin, R. Rong, G. Cao, and Q. Deng, "Prevention of surgical site infection under different ventilation systems in operating room environment," *Frontiers of Environmental Science & Engineering*, vol. 15, no. 3, p. 36, 2021.